International Journal of Marine Engineering Innovation and Research, Vol. 8(2), Jun. 2023. 367-375
(pISSN: 2541-5972, eISSN: 2548-1479)

Influence of Slat Size Variation as Passive Flow Control Instruments on NACA 4415 Airfoil Toward Aerodynamic Performance

James Julian[1], Rizki Aldi Anggara[2], Fitri Wahyuni[3]

(Received: 24 March 2023 / Revised: 20 April 2023 /Accepted: 03 May 2023)

***Abstract*— Airfoil is a fundamental geometry in designing various aerodynamic objects. Passive flow control installation is essential in determining the airfoil's aerodynamic performance. The influence of variations in slat size as a passive flow control instrument is analyzed using the CFD method with a Reynold number of $Re = 10^6$. In this study, NACA 6641 was seleceted as slat. The slat has two variations, i.e., 10% and 16% of the chord length. Based on the computational results, variations in slat size have a substantial influence on the aerodynamic efficiency of the airfoil. Variations in slat size additional C_l ability to reach 20.6043% and 13.1917%, respectively. In addition, a 16%c slat can delay a stall until it reaches AoA ≥ 19°. Meanwhile, a 10%c slat can delay a stall until it reaches AoA ≥ 17°. Variations in slat size also affect the drag force. Slat measuring 16%c can addition C_d up to 50.9252%. Meanwhile, 10% c slat additional C_d up to 21.8389%. Based on the resulting lift-to-drag ratio curve, a 10%c slat has the lowest lift-to-drag ratio compared to a 16%c slat. However, a 10%c slat has the highest level of stability when compared to a 16%c slat installation and without a slat installation.**

Keywords—airfoil; aerodynamic efficiency; CFD; NACA 4415

I. INTRODUCTION[1]

The airfoil can be defined as a geometric design designed to produce a lift force more substantial than the drag force as an aerodynamic efficiency. The resulting aerodynamic efficiency is highly dependent on the geometry of the airfoil. Airfoils generally have many applications in designing aerodynamic objects, such as airplane wings and wind turbine blades [1], [2]. Based on its aerodynamic characteristics, each type of airfoil has specific properties when interacting with fluid flow. The stall is a phenomenon that is avoided in designing airfoils [3]. Stalls form when excessive flow separation occurs. This phenomenon results in a loss of lift ability on the airfoil. In designing airfoils, installing passive flow control instruments is a form of modification to overcome flow separation. Installing a slat around the airfoil's leading-edge is one of the passive flow control instruments. Slat installation has the property of suppressing fluid flow on the top side of the airfoil [4] – [8]. Therefore, the installation of slats as passive flow control has been developed to date.

There is research that discusses the influence of installing a leading-edge slat on aerodynamic efficiency of wind turbines. A study explicitly discusses slat installation's influence on the airfoil's aerodynamic efficiency. The influence of slat on the aerodynamics of the S809 airfoil and the phase IV blade was analyzed. The conclusion obtained based on one of the cases conducted shows that the installation of slat substantially influences the aerodynamic efficiency of the S809 airfoil and the phase IV blade. In this case, the flow separation points at AoA=16.22° locomoted from x/c = 0.47 to 0.67 and additional the coefficient of lift by 52.99% [9]. In addition, other studies discuss the computational evaluation of the optimal leading-edge slat deflection angle to control the dynamic stall of vertical axis wind turbines at low wind speeds. The simulation process was carried out in 2D through the unsteady Reynolds-averaged Navier-Stokes (URANS) numerical approach and applying the sliding mesh technique in Ansys Fluent. This study's conclusion shows a reduction in the optimum deflection angle from 16° at a wind velocity of 10 m/s to 12° at a low wind velocity of 5 m/s. An addition in the maximum lift coefficient of around 32% and the AoA stall can be delayed up to 3° [10].

In addition, other studies discuss the characteristics of single-slat and double-slat installation on NACA 4415 airfoil. This study varies the number of slats with a Reynolds number of $Re = 3\times10^6$ to be analyzed. The type of slat used was Eppler 421. The conclusion of this study showed that the installation of variations in the number of slats could enhance the aerodynamic efficiency of the airfoil. Single-slat and double-slat installations could delay the stall from 16° to 20°. The magnitude of the addition in the lift coefficient on single slats and double slats is not much different. However, single slats can create a more favorable lift-to-drag ratio than double slats [11].

This study analyzed the influence of installing slats as passive flow control instruments on the aerodynamic efficiency of the NACA 4415 airfoil. The slat used is NACA 6411. The study was performed operating the computational fluid dynamic (CFD) method. installing

James Julian, Department of Mechanical Engineering, Universitas Pembangunan Nasional Veteran Jakarta, Jakarta, 12450, Indonesia. E-mail: zames@upnvj.ac.id
Rizki Aldi Anggara, Department of Mechanical Engineering, Universitas Pembangunan Nasional Veteran Jakarta, Jakarta, 12450, Indonesia. E-mail: rizky.aldianggara06@gmail.com
Fitri Wahyuni, Department of Mechanical Engineering, Universitas Pembangunan Nasional Veteran Jakarta, Jakarta, 12450, Indonesia. E-mail: fitriwahyuni@upnvj.ac.id

passive flow control instruments is susceptible to location, size, and geometric shape. So, research on passive flow control instruments still needs to be developed to achieve maximum efficiency. Thus, this study was developed by varying the size of the slat geometry at predetermined locations as a comparison based on the slat size that has the best efficiency level on airfoil aerodynamic efficiency.

II. METHOD

A. NACA 4415

NACA 4415 airfoil is the object developed by the National Advisory Committee for Aerodynamics (NACA) chosen in this study to analyze its aerodynamics [12] – [14]. The characteristics of NACA 4415 can be seen from the digits. NACA 4415 airfoil is an asymmetrical airfoil type with a top chamber of 4% chord length (c) located at 40%c and has a maximum airfoil thickness of 15%c. With these characteristics, the NACA 4415 airfoil can addition lift quite well, even in conditions of unstable fluid flow [15]. The NACA 4415 airfoil chord length used in this study is 1m.

Figure 1. Airfoil NACA 4415

B. Geometries

This study conducted variations in slat size to analyze their influence on the aerodynamic efficiency of the airfoil. There were three samples used as data to be analyzed in this study. The first sample is without a slat as the research baseline; the second is with a 10% c slat; the third is with a slat of 16% c. The type of slat used in this study is NACA 6411, located around the leading-edge. Based on the coordinates of the points, the slat is located at coordinates y=0.165 with a deflection angle of -20°. The three samples are in the fluid domain, combining semicircles and squares. Sample details and fluid domains can be seen in Figure 2.

C. Numerical Method and Turbulence Model

Numerical methods are used to determine research data. This numerical method uses the Reynolds Averaged Navier-Stokes (RANS) equation. It equation is a modified equation for CFD applications [16], [17]. Mathematically, equations (1) and (2) represent the RANS equation. Both of these equations include continuity equations of fluid flow and momentum flow.

$$\frac{\partial \rho}{\partial t} + \frac{\partial}{\partial x_i}(\rho u_i) = 0 \tag{1}$$

$$\frac{\partial}{\partial t}(\rho u_i) + \frac{\partial}{\partial x_i}(\rho u_i u_j) = \frac{\partial p}{\partial x_i} + \frac{\partial}{\partial x_j}\left[\mu\left(\frac{\partial u_i}{\partial x_j} + \frac{\partial u_j}{\partial x_i} - \frac{2}{3}\delta_{ij}\frac{\partial u_i}{\partial x_i}\right)\right] + \frac{\partial}{\partial x_i}\left(-\rho\overline{u_i' u_j'}\right) \tag{2}$$

The k-ε model is used in solving computations numerically as a turbulence model. This turbulence model is commonly used in CFD applications. Besides being a simple turbulence model, the turbulence model has a good level of accuracy and is affordable. The k-ε turbulence model includes the equation for the dissipation rate and the kinetic energy of the turbulence [18] – [22]. The equation of the k-ε turbulence model is shown in equations (3) and (4).

$$\frac{D}{Dt}(\rho k) = \frac{\partial}{\partial x_j}\left[\left(\mu + \frac{\mu_t}{\sigma_k}\right)\frac{\partial k}{\partial x_j}\right] + G_k - \rho\varepsilon \tag{3}$$

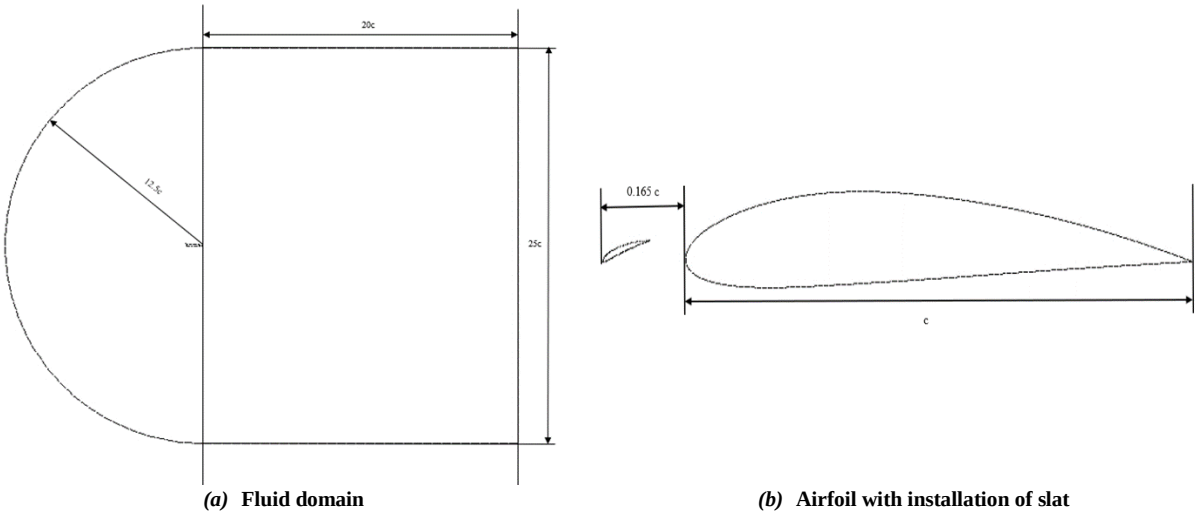

(a) **Fluid domain** ***(b)*** **Airfoil with installation of slat**

Figure 2: Detail geometries

$$\frac{D}{Dt}(\rho\varepsilon) = \frac{\partial}{\partial x_j}\left[\left(\mu + \frac{\mu_t}{\sigma\varepsilon}\right)\frac{\partial\varepsilon}{\partial x_j}\right] + C_{el}\frac{\varepsilon}{k}G_k - \rho C_{\varepsilon 2}\frac{\varepsilon^2}{k} \quad (4)$$

D. Meshing and boundary condition

In the computational process, this study uses an unstructured mesh. The geometry of the mesh operated is triangular. The Reynolds number is defined as the boundary condition of $\mathrm{Re} = 10^6$. In the fluid domain, two boundary conditions are established. The first boundary condition is velocity-inlet with a velocity magnitude of 14.77 m/s, and the second boundary condition is zero pressure outlet. In addition, the boundary conditions are also specified on the airfoil and slat as a stationary wall (no slip). Detailed mesh and boundary conditions can be seen in Figure 3.

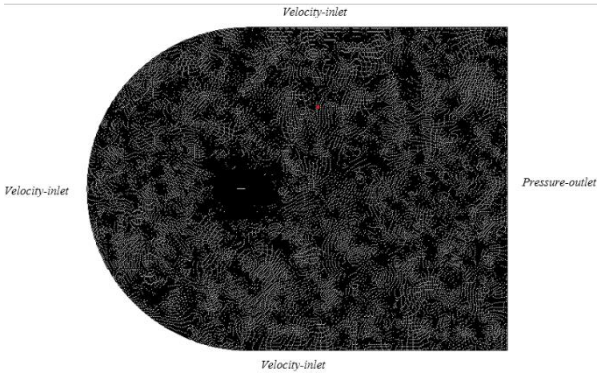

Figure 3: Mesh and boundary condition

E. Grid independency study

This study has three types of mesh variations based on the number of elements. Figure 4 show the variation of mesh, including fine mesh (202368 elements), medium mesh (162768 elements), and coarse mesh (130277 elements). A grid independence study of the three variations was conducted to determine the type of mesh to use based on the lowest error rate. Thus, the computational process can be carried out optimally based on accuracy.

This grid independence study was based on Richardson's extrapolation [23]. The fluid flow velocity at x = 0.5 and y = 0.15 is determined as a sample for each mesh in the grid independence study process. The initial step is determined by the ratio of grid variations and order values using equations (5) and (6). Next, determine the Grid Convergence Index (GCI), which is calculated using equations (7) and (8). There are two types of GCIs used. The first GCIs are GCI_{fine}, the error value generated between fine and medium mesh. While the second GCIs is GCI_{coarse} which is the error value generated between medium and coarse mesh. The GCI that has been determined is analyzed with equation (9) to ensure the mesh variations are in the convergence region. Each mesh can calculate its error value with equation (10) as a final step. The fine mesh has the lowest error rate based on the calculation results. Thus, the fine mesh will be utilized as a mesh in computing. Table 1 shows the results of the grid independence study.

$$r = \frac{h_2}{h_1} \quad (8)$$

$$\bar{p} = \frac{\ln\left(\frac{f_3 - f_2}{f_2 - f_1}\right)}{\ln(r)} \quad (9)$$

$$GCI_{fine} = \frac{F_s\,|\in|}{\left(r^{\bar{p}} - 1\right)} \quad (10)$$

$$GCI_{coarse} = \frac{F_s\,|\in|\,r^{\bar{p}}}{\left(r^{\bar{p}} - 1\right)} \quad (11)$$

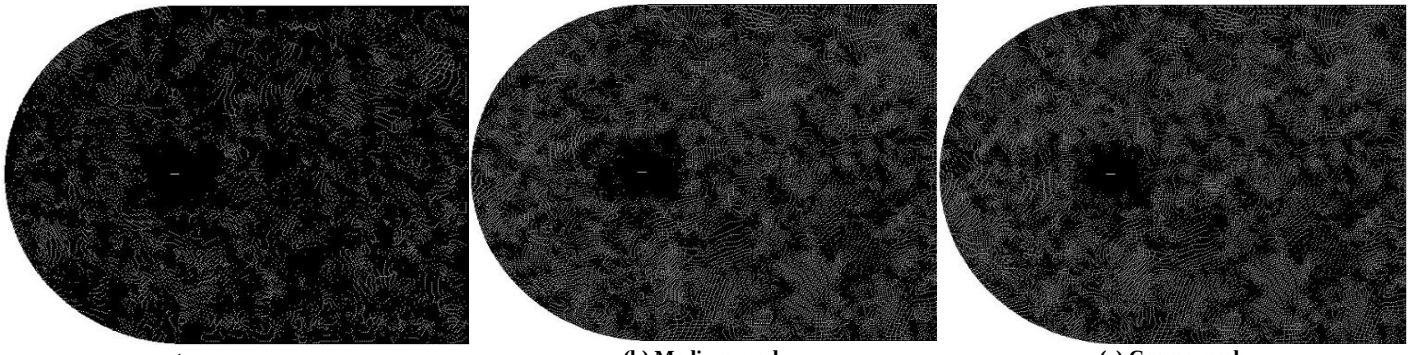

(a) Fine mesh **(b) Medium mesh** **(c) Coarse mesh**

Figure 4: Variations of mesh

$$\in = \frac{f_{n+1} - f_n}{f_n} \quad (12)$$

$$\frac{GCI_{coarse}}{GCI_{fine} r^{\bar{p}}} \approx 1 \quad (13)$$

$$f\,\mathrm{r}_{h=0} = f_1 + \frac{(f_1 - f_2)}{\left(r^{\bar{p}} - 1\right)} \quad (14)$$

TABLE 2.
GRID INDEPENDENCY STUDY RESULT

Mesh	Fine	Medium	Coarse
Velocity	16.2648	16.301	16.3995
$\bar{\bar{p}}$		4.485890018	
r		1.25	
GCI_{fine}		0.161%	
GCI_{coarse}		0.4389%	
$f_{rh} = 0$		16.24376565	
$\frac{GCI_{coarse}}{GCI_{fine} r^{\bar{\bar{p}}}}$		1.00187	
Error	0.12949%	0.35235%	0.95873%

III. Results and Discussion

A. Validation

Before conducting data analysis, the research data obtained was first validated. The results of the computational data are validated with the results of experimental data conducted by Hoffman as a comparison [24]. This validation aims to ensure that the computational data results conform with the actual fluid flow conditions. The sample used for comparison is the data coefficient of lift (C_l) and coefficient of drag (C_d) on the airfoil without slat (baseline) generated by computational results and experimental results on the Reynolds number set at $\mathrm{Re} = 10^6$. The first validation carried out was C_l on computational and experimental data, as shown in Figure 5a. In Figure 5a, the C_l curve shown in the computational and experimental data differs. The C_l data obtained in the experiment is higher than the computational results. The difference begins to be seen clearly at the peak of the C_l curve of the two data. In addition, the stall phenomenon in the computational data occurs earlier at AoA 15° than in the experimental data, which occurs at AoA 17°. However, the trends shown from the two curves show similarities. The two curves show that as AoA additions in the airfoil, C_l also additions in the curve and a substantial reduction in C_l occurs when the airfoil experiences a stall.

Furthermore, the second validation carried out was C_d on computational and experimental data, as shown in Figure 5b. Figure 5b shows that the computational and experimental data C_d curves are identical. In addition, the trend shown in the computational and experimental data shows that the higher the AoA in the airfoil, the more significant the C_d created. Thus, the data generated based on computational results have valid results.

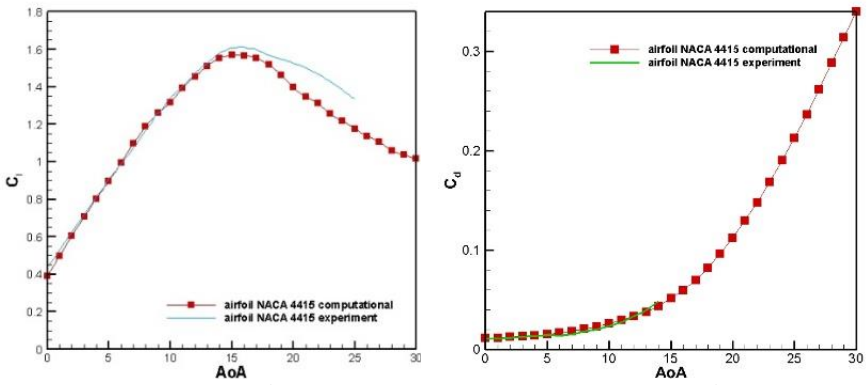

(a) Graph of C_l (b) Graph of C_d

Figure 5: Validation graph of C_l and C_d

B. Analysis

This study analyzed the influence of installing slats on the aerodynamic efficiency of the NACA 4415 airfoil. Variation of slat size was operated as a passive flow control instrument to show the most influential slat size. Based on the computational results obtained, installing slats can add to the ability of the airfoil to generate lift. Figure 6a shows that an airfoil with a 16% c slat installation can generate higher lift forces than a 10% c slat installation. A substantial addition in C_l in both slats begins to be seen when AoA ≥ 5°. Installation of slats around the leading-edge of the airfoil can provide a good flow influence in producing lift. The predetermined gap between the slats at a certain deflection angle with the airfoil can add fluid flow velocity on the top side of the airfoil. This phenomenon follows Bernoulli's principle; an addition in velocity on the top side of the airfoil provides low pressure. The pressure drop on the top side of the airfoil provides a high-pressure difference with the pressure on the bottom

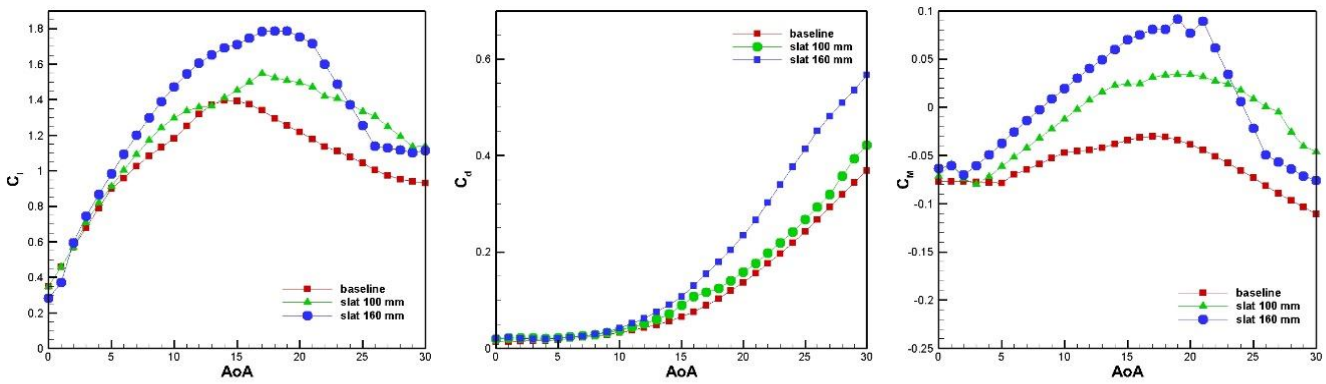

(a) Graph of C_l (b) Graph of C_d (c) Graph of C_M

Figure 6: Aerodynamic efficiency of airfoil parameters

side of the airfoil so that it can add to the airfoil's ability to generate lift.

In addition, the slats can suppress fluid flow so that fluid can continue to flow on the top side of the airfoil. The influence of this phenomenon can be seen in the installation of slats that flow separation can be minimized to delay stalls. Stall occurs in the airfoil airfoil impacts the resulting drag. Figure 6b shows a substantial addition in C_d in the airfoil with the slat installation. C_d additions continuously with the addition in AoA. The addition in C_d occurs due to recirculation in the fluid flow. Flow recirculation occurs in the vacuum area formed by flow separation. The vacuum area formed gives the influence of a thrust force on the

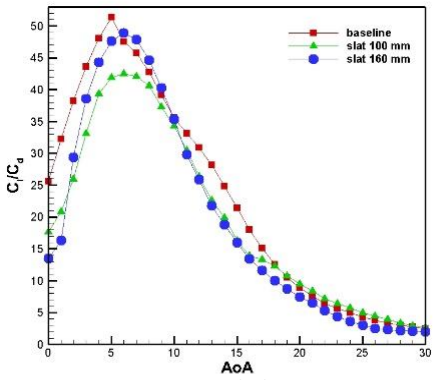

Figure 7. Graph of lift-to-drag ratio

without slat installation at AoA ≥ 15°. By installing 10%c slats, the stall can be delayed up to AoA ≥ 17°. In installing a 16%c slat, the stall can be delayed up to AoA ≥ 19°. Based on the average percentage addition in C_l obtained in Table 2, a 10% c slat can addition C_l on average to 13.1917%. At a 16% c slat, the average percentage addition in C_l can addition to 20.6043%.

Besides increasing lift, the installation of slats on the airfoil, which inhibits the airfoil aerodynamically. More specifically, in table 2, the average percentage addition in C_d shows that installing a 10%c slat can addition the average C_d to 21.8389%. Meanwhile, in installing 16%c slat, the average addition was more substantial, up to 50.9252%.

C_M data is shown in Figure 6c as a dimensionless parameter in identifying the stability of the airfoil

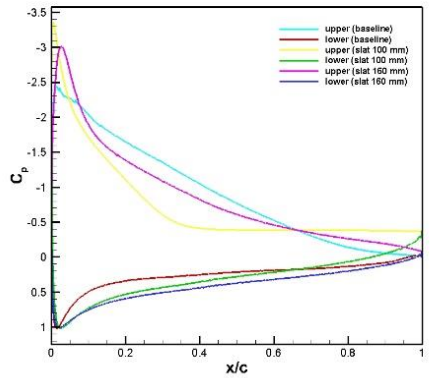

Figure 8. Graph of C_P

against the installation of 10%c slat and 16%c slat. The torque value of the total force acting on the airfoil is used to determine the stability level. The resulting torque value will affect the stability of the airfoil through the pitching moment. Pitch-up is a phenomenon of the tendency of the airfoil to experience a clockwise torque

generated when C_M is positive. Conversely, pitch-down shows the phenomenon of the tendency of the airfoil to experience a counterclockwise torque when the resulting C_M is negative. Based on the resulting C_M, the airfoil can be stable when the obtained C_M is zero. It can be seen in Figure 6c that installing slats can affect the stability of the airfoil. In an airfoil without slat installation, the resulting C_M is dominantly negative, so the torque's tendency is in the form of pitch-down. Even so, there is an addition in the value of C_M close to zero with an addition in AoA. It indicates that airfoil stability additions when the AoA additions before a stall. In the installation of slats around the leading-edge of the airfoil, the resulting C_M tends to addition until it reaches a positive C_M value. The most substantial C_M addition was obtained in installing a 16% c slat. However, the increasing substantial value of C_M will disturb the stability of the airfoil. Another thing happened in the installation of a 10% c slat. Although the resulting C_M can reach positive C_M, the curve shown along with the addition in AoA is more sloping. It shows that the installation of a 10% c slat has a better level of stability.

The aerodynamic efficiency of an airfoil is good when it can produce maximum lift with minimum drag. In Figure 7, the lift-to-drag ratio is shown to compare the aerodynamic efficiency of the airfoil without slat installation and with slat installation. In Figure 7 show that when installing the slat, there is a decrease in the lift-to-drag ratio. When AoA ≤ 3°, the lowest lift-to-drag ratio is obtained on the airfoil with 16% c slat installation. However, the lift-to-drag ratio resulting in this installation additions compared to the installation of a 10%c slat at AoA ≤ 3°. The resulting trend curve for 16% c slat installation is getting closer to the airfoil efficiency without slat installation. Thus, the lift-to-drag ratio shows that the airfoil with a slat installation of 16%c shows better aerodynamic efficiency than the installation of a 10%c slat.

To further analyze the role of slat installation around the airfoil's leading edge, the pressure coefficient distribution along the airfoil chord is shown at the condition AoA= 20°. The high AoA shown aims to demonstrate the ability of the slat to suppress recirculation in the fluid flow, which additions with the addition in AoA. In the previous discussion, the three airfoil samples showed a stall condition. In these conditions, the airfoil no longer produces lift due to the flow separation that occurs. Figure 8 show that the slat's ability to overcome flow recirculation in flow separation affects the pressure distribution that occurs in the airfoil. Substantial differences can be seen on the top side of the airfoil.

TABLE 2.
AVERAGE PERCENTAGE ADDITION IN C_L AND C_D OF 10%C SLAT AND 16%C SLAT

percentage	C_l		C_d	
	100	160	100	160
0	0,0663%	-19,1580%	45,0214%	53,0937%
1	0,1747%	-18,9598%	55,0081%	60,1594%
2	-0,0087%	4,6790%	47,4119%	36,3632%
3	3,8388%	9,3029%	36,7937%	23,4399%
4	3,5005%	9,5095%	26,3073%	18,6507%
5	1,3044%	9,0669%	24,1822%	17,7323%
6	4,7963%	14,2865%	17,2417%	11,2284%
7	6,6416%	17,0721%	15,8742%	11,8385%
8	8,2388%	19,7552%	13,9741%	14,7363%
9	9,7344%	22,5854%	15,3846%	19,3008%
10	9,9963%	24,5613%	14,0038%	25,6508%
11	6,8665%	23,4758%	15,9779%	37,2523%
12	2,7929%	21,5776%	20,2502%	45,2884%
13	-0,4378%	20,4052%	24,1356%	56,2344%
14	1,1012%	21,2797%	26,4088%	60,9856%
15	4,3520%	22,7143%	8,8983%	64,6224%
16	9,2563%	27,2413%	41,6902%	70,9766%
17	15,5396%	33,2692%	30,3019%	73,4405%
18	17,8226%	38,0851%	19,8691%	73,5826%

19	20,3393%	42,3931%	17,4488%	71,2234%
20	22,7253%	43,7231%	15,4597%	72,1732%
21	24,9704%	45,8777%	13,4884%	70,8486%
22	24,9506%	41,0258%	12,0909%	72,0264%
23	26,9302%	33,8475%	11,2807%	73,1439%
24	27,8950%	27,0998%	10,4252%	72,3879%
25	27,7960%	20,0708%	10,3420%	71,1518%
26	30,2345%	13,4886%	9,4954%	68,4782%
27	28,4360%	16,0285%	8,8098%	63,8338%
28	25,3783%	17,3265%	12,0793%	59,4911%
29	21,0376%	17,3230%	14,5246%	55,7217%
30	22,6732%	19,7786%	14,4181%	53,6254%
average	13,1917%	20,6043%	20,9225%	50,9252%

The pressure distribution that occurs in each airfoil shows different conditions. In an airfoil without a slat installation, the stall occurs earlier than in an airfoil with a slat installation. The difference in pressure distribution is visible around the airfoil's leading edge. With the installation of slats, there is a pressure drop, especially in the installation of 16% c slats. In the airfoil with 16% c slat installation, a new stall begins to occur, which results in turbulent flow around the leading edge of the airfoil before finally flowing to the airfoil's trailing edge and causing a substantial reduction in lift. The drop pressure shown on the airfoil with the slat installation can be identified as a form of the slat's ability to delay the stall in the airfoil by suppressing the recirculating fluid flow on the top side the airfoil.

Visualization of the fluid flow that interacts around the airfoil with and without slat installation is displayed when AoA= 20°. The visualization shown includes the contour velocity magnitude, pressure, and streamline, as seen in Figure 9. In Figure 9, it can be seen that the airfoil has a high AoA. The airfoil is in a stall condition due to the flow separation, thus forming an enlarged fluid flow recirculation. Based on Figure 9, it is evident that the airfoil with the slat installation around the leading edge can suppress the recirculation of fluid flow. Recirculation of fluid flow is suppressed to direct fluid flow so that it can flow appropriately following the shape of the airfoil surface. The slat can suppress the fluid flow in the airfoil quite well by installing a 10% c slat. A 10% c slat can minimize fluid flow recirculation so that stall conditions can be delayed. In addition, fluid flow can also be suppressed by a 16% c slat. A 16% c slat can minimize fluid flow recirculation very well. It can be seen that there is no fluid flow recirculation that occurs in the airfoil. This capability proves that a 16% c slat has a better ability than a 10% c slat in enhancing the aerodynamic efficiency of the airfoil, especially the slat's ability to delay the stall on the airfoil. However, there is a more substantial recirculation of fluid flow at 16% c slats. However, these conditions did not substantially impact the aerodynamic efficiency of the airfoil.

IV. CONCLUSION

This study analyzed the influence of installing various slat sizes on the aerodynamic efficiency of NACA 4415 airfoils. The type of slat used was NACA 6411 airfoil with two size variations, namely 10%c and 16%c. Based on the computational results obtained, the installation of slats on the airfoil can addition the ability of the airfoil to generate lift. The airfoil installing a 16% c slat can addition the ability to produce C_l on average up to 20.6043%. Meanwhile, installing a 10% c slat can addition the average C_l to 13.1917%. In addition, the stall condition on the airfoil with the slat installation can be delayed. A 16%c slat can delay a stall until it reaches AoA $\geq$ 19°. Whereas in the installation of sized slats, it can delay stalls until it reaches AoA $\geq$ 17°. Under these conditions, a 16%c slat can produce lift better than a 10%c slat. As a result of the larger size, the gap between the airfoil and the slat will be smaller to addition the velocity of fluid flow on the top side of the airfoil to minimize the recirculation of fluid flow that occurs. However, the C_d produced in the airfoil with slat installation additional more substantially than in the airfoil without slat installation. The addition in C_d occurred in the airfoil with the installation of a 16% c slat of 50.9252%. Meanwhile, at 10% c slat, C_d additional by 21.8389%. These conditions cause the lift-to-drag ratio on the airfoil with the slat installation to reduction due to the excessive addition in C_d. So the aerodynamic efficiency of the airfoil is not optimal. However, installing a 16%c slat has better aerodynamic efficiency than installing a 10%c slat.

The installation of slat size variations on the airfoil can also affect the stability of the airfoil. A slat size that is too large can interfere with the stability of the airfoil. Based on the resulting C_M, installing a 10% c slat can improve the stability of the airfoil properly. However, there was a substantial addition in C_M on the airfoil with 16% c slat installation. Based on fluid flow visualization around the airfoil, the installation of slats on the airfoil can suppress the recirculation of fluid flow. Due to its larger size, a 16%c slat can better suppress fluid flow than a 10%c slat so that the fluid can flow through the airfoil properly.

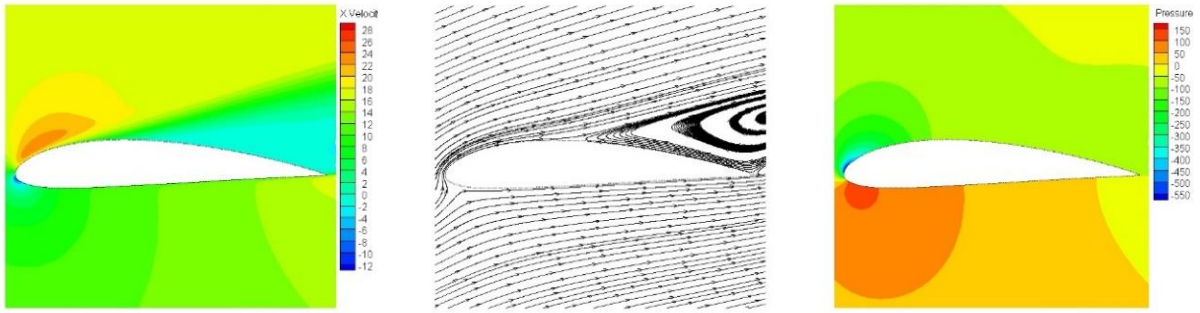

(a) NACA 4415 (baseline) (b) NACA 4415 (baseline) (c) NACA 4415 (baseline)

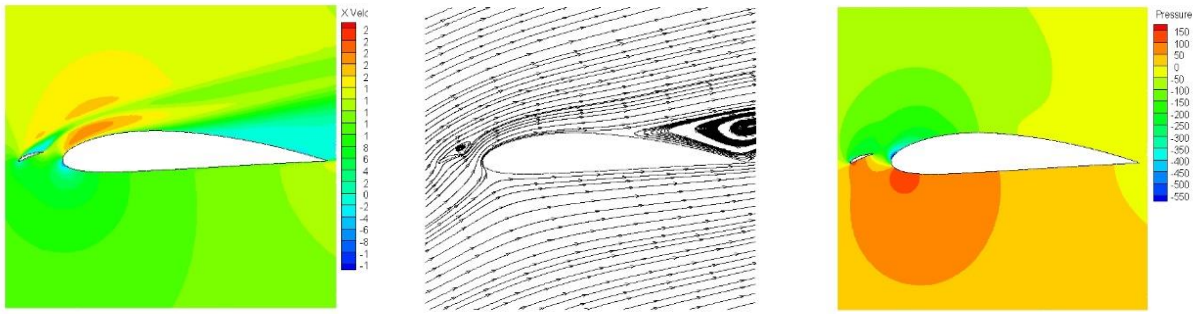

(d) NACA 4415 with 10% c slat (e) NACA 4415 with 10% c slat (f) NACA 4415 with 10% c slat

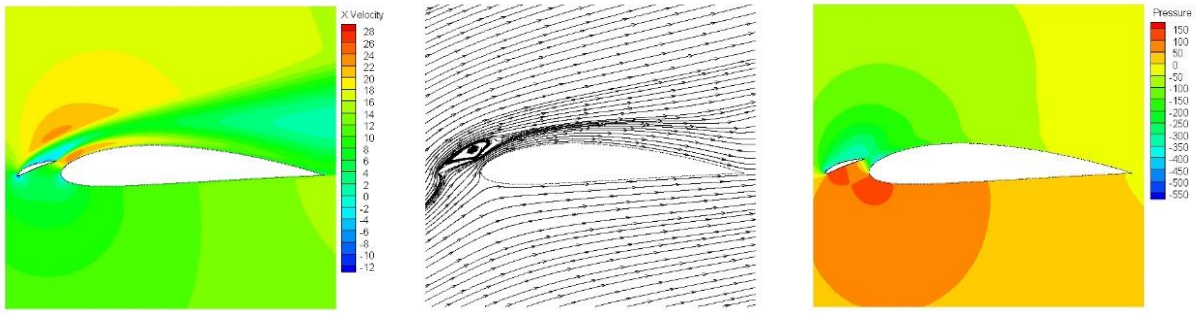

(g) NACA 4415 with 16% c slat (h) NACA 4415 with 16% c slat (i) NACA 4415 with 16% c slat

Figure 9. Magnitude velocity, streamlines contour, and pressure contour at AoA=20°

REFERENCES

[1] J. G. Coder and D. M. Somers, "Design of a slotted, natural-laminar-flow airfoil for commercial transport applications," *Aerosp Sci Technol*, vol. 106, p. 106217, 2020, doi: https://doi.org/10.1016/j.ast.2020.106217.

[2] S. Huang, H. Qiu, and Y. Wang, "Aerodynamic efficiency of horizontal axis wind turbine with application of dolphin head-shape and lever movement of skeleton bionic airfoils," *Energy Convers Manag*, vol. 267, p. 115803, 2022, doi: https://doi.org/10.1016/j.enconman.2022.115803

[3] S. Le Fouest, J. Deparday, and K. Mulleners, "The dynamics and timescales of static stall," *J Fluids Struct*, vol. 104, p. 103304, 2021.

[4] C. Tung, K. W. McAlister, and C. M. Wang, "Unsteady aerodynamic behavior of an airfoil with and without a slat," *Comput Fluids*, vol. 22, no. 4–5, pp. 529–547, 1993.

[5] M. D. Kesuma, R. Irwansyah, J. Julian, and A. Satyadharma, "Flow Control with Multi-DBD Plasma Actuator on a Delta Wing," 2020.

[6] Harinaldi, A. S. Wibowo, J. Julian, and Budiarso, "The comparison of an analytical, experimental, and simulation approach for the average induced velocity of a dielectric barrier discharge (DBD)," in *AIP Conference Proceedings*, 2019, vol. 2062, no. 1, p. 020027.

[7] F. C. Megawanto, Harinaldi, Budiarso, and J. Julian, "Numerical analysis of plasma actuator for drag reduction and lift enhancement on NACA 4415 airfoil," in *AIP Conference Proceedings*, 2018, vol. 2001, no. 1, p. 050001.

[8] J. Julian, W. Iskandar, F. Wahyuni, and N. T. Bunga, "Characterization of the Co-Flow Jet Effect as One of the Flow Control Devices," *Jurnal Asiimetrik: Jurnal Ilmiah Rekayasa & Inovasi*, pp. 185–192, 2022.

[9] H. Wang *et al.*, "Effects of leading edge slat on flow separation and aerodynamic efficiency of wind turbine," *Energy*, vol. 182, pp. 988–998, 2019.

[10] T. Ullah, A. Javed, A. Abdullah, M. Ali, and E. Uddin, "Computational evaluation of an optimum leading-edge slat deflection angle for dynamic stall control in a novel urban-scale vertical axis wind turbine for low wind speed operation," *Sustainable Energy Technologies and Assessments*, vol. 40, p. 100748, 2020.

[11] J. Julian, W. Iskandar, F. Wahyuni, A. Armansyah, and F. Ferdyanto, "Effect of Single Slat and Double Slat on Aerodynamic Efficiency of NACA 4415," *International Journal of Marine Engineering Innovation and Research*, vol. 7, no. 2, 2022.

[12] R. I. Rubel, M. K. Uddin, M. Z. Islam, and M. Rokunuzzaman, "Comparison of Aerodynamics Characteristics of NACA 0015 & NACA 4415," 2016.

[13] M. J. Hoffmann, R. Reuss Ramsay, and G. M. Gregorek, "Effects of grit roughness and pitch oscillations on the NACA 4415 airfoil," National Renewable Energy Lab.(NREL), Golden, CO (United States); The Ohio …, 1996.

[14] J. Julian, W. Iskandar, and F. Wahyuni, "Aerodynamics Improvement of NACA 0015 by Using Co-Flow Jet," *International Journal of Marine Engineering Innovation and Research*, vol. 7, pp. 1479–2548, Mar. 2022, doi: 10.12962/j25481479.v7i4.14898.

[15] F. C. Megawanto, R. F. Karim, N. T. Bunga, and J. Julian, "Flow separation delay on NACA 4415 airfoil using plasma actuator effect," *International Review of Aerospace Engineering*, vol. 12, no. 4, pp. 180–186, 2019.

[16] S. M. A. Aftab, A. S. Mohd Rafie, N. A. Razak, and K. A. Ahmad, "Turbulence model selection for low Reynolds number flows," *PLoS One*, vol. 11, no. 4, p. e0153755, 2016.

[17] J. Julian, Harinaldi, Budiarso, C.-C. Wang, and M.-J. Chern, "Effect of plasma actuator in boundary layer on flat plate model with turbulent promoter," *Proc Inst Mech Eng G J Aerosp Eng*, vol. 232, no. 16, pp. 3001–3010, 2018.

[18] M. Ahsan, "Numerical analysis of friction factor for a fully developed turbulent flow using k–ε turbulence model with enhanced wall treatment," *Beni Suef Univ J Basic Appl Sci*, vol. 3, no. 4, pp. 269–277, 2014.

[19] J. Julian, W. Iskandar, and F. Wahyuni, "COMPUTATIONAL FLUID DYNAMICS ANALYSIS BASED ON THE FLUID FLOW SEPARATION POINT ON THE UPPER SIDE OF THE NACA 0015 AIRFOIL WITH THE COEFFICIENT OF FRICTION," *Jurnal Media Mesin*, vol. 23, no. 2.

[20] Harinaldi, Budiarso, and J. Julian, "The effect of plasma actuator on the depreciation of the aerodynamic drag on box model," in *AIP Conference Proceedings*, 2016, vol. 1737, no. 1, p. 040004.

[21] J. Julian, R. Difitro, and P. Stefan, "The effect of plasma actuator placement on drag coefficient reduction of Ahmed body as an aerodynamic model," *International Journal of Technology*, vol. 7, no. 2, pp. 306–313, 2016.

[22] J. Julian, W. Iskandar, F. Wahyuni, and N. T. Bunga, "Aerodynamic Efficiency Improvement on NACA 4415 Airfoil by Using Cavity," *Jurnal Asiimetrik: Jurnal Ilmiah Rekayasa Dan Inovasi*, vol. 5, no. 1, Jan. 2023, doi: 10.35814/asiimetrik.v5i1.4259.

[23] P. J. Roache, "Perspective: a method for uniform reporting of grid refinement studies," 1994.

[24] M. J. Hoffmann, R. Reuss Ramsay, and G. M. Gregorek, "Effects of grit roughness and pitch oscillations on the NACA 4415 airfoil," National Renewable Energy Lab.(NREL), Golden, CO (United States); The Ohio …, 1996.